

Observation of unsaturated platinum carbenes $\text{Pt}_2\text{C}_{2n}^-$ ($n = 1-3$) clusters: A photoelectron imaging spectroscopic and theoretical study

Cite as: J. Chem. Phys. **156**, 164302 (2022); <https://doi.org/10.1063/5.0079854>

Submitted: 25 November 2021 • Accepted: 05 April 2022 • Accepted Manuscript Online: 06 April 2022

• Published Online: 25 April 2022

Xuegang Liu,  Gang Li,  Zhiling Liu, et al.



View Online



Export Citation



CrossMark

ARTICLES YOU MAY BE INTERESTED IN

[A deep potential model with long-range electrostatic interactions](#)

The Journal of Chemical Physics **156**, 124107 (2022); <https://doi.org/10.1063/5.0083669>

[Photoelectron imaging of \$\text{PtI}_2^-\$ and its \$\text{PtI}^-\$ photodissociation product](#)

The Journal of Chemical Physics **156**, 134303 (2022); <https://doi.org/10.1063/5.0085610>

[An ion mobility mass spectrometer coupled with a cryogenic ion trap for recording electronic spectra of charged, isomer-selected clusters](#)

Review of Scientific Instruments **93**, 043201 (2022); <https://doi.org/10.1063/5.0085680>

Lock-in Amplifiers
up to 600 MHz



Zurich
Instruments



Observation of unsaturated platinum carbenes $\text{Pt}_2\text{C}_{2n}^-$ ($n = 1-3$) clusters: A photoelectron imaging spectroscopic and theoretical study

Cite as: J. Chem. Phys. 156, 164302 (2022); doi: 10.1063/5.0079854

Submitted: 25 November 2021 • Accepted: 5 April 2022 •

Published Online: 25 April 2022



View Online



Export Citation



CrossMark

Xuegang Liu,^{1,2} Gang Li,² Zhiling Liu,³ Jinghan Zou,² Dong Yang,² Shihu Du,² Wenshao Yang,^{1,a)} Ling Jiang,^{2,a)} and Hua Xie^{2,a)}

AFFILIATIONS

¹ Hangzhou Institute of Advanced Studies, Zhejiang Normal University, 1108 Gengwen Road, Hangzhou 311231, Zhejiang, China

² State Key Laboratory of Molecular Reaction Dynamics, Dalian Institute of Chemical Physics, Chinese Academy of Sciences, 457 Zhongshan Road, Dalian 116023, Liaoning, China

³ School of Chemical and Material Science, Key Laboratory of Magnetic Molecules and Magnetic Information Materials, Ministry of Education, Shanxi Normal University, 339 Taiyu Road, Taiyuan, Shanxi 030000, China

^{a)} Authors to whom correspondence should be addressed: wenshaoyang@zjnu.cn; ljiang@dicp.ac.cn; xiehua@dicp.ac.cn

ABSTRACT

The structural and bonding properties of the $\text{Pt}_2\text{C}_{2n}^-$ ($n = 1-3$) complexes have been investigated by mass-selected photoelectron velocity-map imaging spectroscopy with quantum chemical calculations. The adiabatic detachment energies and vertical detachment energies of $\text{Pt}_2\text{C}_{2n}^-$ have been obtained from the measured photoelectron imaging spectra. Theoretical results indicate that the lowest-energy isomers of $\text{Pt}_2\text{C}_{2n}^-$ ($n = 1-3$) possess linear chain-shaped configurations. The binding motif in the most stable isomer of Pt_2C_2^- has a linear cumulenic structure with a $\text{Pt}=\text{C}=\text{C}=\text{Pt}$ configuration, and the structural characteristic persists up to all the lowest-energy isomers of the Pt_2C_4^- and Pt_2C_6^- anions. The chemical bonding analyses indicate that the $\text{Pt}_2\text{C}_{2n}^-$ ($n = 1-3$) complexes have multicenter two-electron characteristics.

Published under an exclusive license by AIP Publishing. <https://doi.org/10.1063/5.0079854>

INTRODUCTION

Supported noble metal catalysts are widely applied in the current industrial catalysis. Since the Pt_1/FeO_x single-atom catalysts were first reported,¹ the proposed “single-atom-catalysis” has rapidly become the forefront in the field of catalytic research.^{2,3} Many transition-metal (i.e., Pd, Pt, and Au) nanoparticles (NPs) have been developed and used in various catalytic processes.⁴⁻⁷ Like a typical noble metal, Pt has many empty d orbitals, which is capable of drawing various electron-rich compounds.⁸ Hence, the Pt-containing compounds could serve as an ideal model when exploring the C-H bond activation and C-C bond formation in cross coupling reactions.^{9,10}

During the past few decades, the noble metal carbide clusters have gained extensive interest in various kinds of experimental and theoretical studies in the gas phase.¹¹⁻²³ For example, PtC_3 and

PdC_3 ¹² were clarified to have linear structures with the $C_{\infty v}$ symmetry, which were different from AuC_3 .¹³ Similar studies of AuC_n^- ($n = 2, 4, \text{ and } 6$) revealed that the AuC_2^- complex has a linear structure, in contrast to the bent geometries of both AuC_4^- and AuC_6^- .¹⁴⁻¹⁶ As for neutral PdC_n , the linear structures are favored when $n = 2-9$, while the cyclical structures are preferred in PdC_n ($n = 10-12$).¹⁷ Density functional theory (DFT) calculations predicted that the whole series of anionic and neutral $\text{Pt}_n\text{C}_2^{-/0}$ ($n = 1-7$) clusters exhibit two-dimensional (2D) planar chain-shaped or ring-based structures.^{21,22} The Pt_2C^- cluster was characterized to have a C_{2v} symmetric Pt-C-Pt bent structure using photoelectron spectroscopy (PES) and DFT calculations.²³ In the binuclear Au_2C_n^- ($n = 2, 4, \text{ and } 6$) complexes, the most stable structure of Au_2C_2^- was identified to have a linear acetylenic $\text{Au}-\text{C}\equiv\text{C}-\text{Au}^-$ configuration, whereas Au_2C_n^- ($n = 4 \text{ and } 6$) were determined to have asymmetric $\text{Au}-\text{Au}-(\text{C}\equiv\text{C})_m^-$ ($m = 2-3$) structures.¹⁸ However, experimental

investigations of binuclear $\text{Pt}_2\text{C}_{2n}^-$ clusters remain elusive thus far. In this work, we report a photoelectron velocity-map imaging spectroscopic study on the series of $\text{Pt}_2\text{C}_{2n}^-$ ($n = 1-3$) species. Quantum chemical calculations have been performed on these clusters to identify the structure of the low-lying isomers and to assign the observed spectral features.

METHODS

Experimental methods

This work was performed using a homemade dual-channel time-of-flight mass spectrometer, coupled with a laser vaporization supersonic cluster source and a photoelectron velocity map imaging analyzer.²⁴ The $\text{Pt}_2\text{C}_{2n}^-$ ($n = 1-3$) anions were produced via laser vaporization of the platinum-carbon mixture target (mole ratio, M/C = 1:5) in expansions of pure helium carrier gas. The cooled clusters of ~ 200 K were then skimmed into the extraction zone of a Wiley-McLaren TOF mass spectrometer. The anions of interest were mass-selected and interacted with laser beams of both 266 nm (4.661 eV) and 355 nm (3.496 eV). The photoelectrons were mapped onto a detector consisting of a micro-channel plate and a phosphor screen and recorded by using a charge-coupled device (CCD) camera. Each raw 2D image was obtained by accumulating 10 000–50 000 laser shots at a 10 Hz repetition rate before being reconstructed using the basis set expansion inverse Abel to transform method (BASEX). The photoelectron spectra were calibrated using the known spectrum of Au^- and have an energy resolution better than 5% (50 meV for 1 eV kinetic energy electrons).

Theoretical details

To elucidate the electronic and geometrical structures of $\text{Pt}_2\text{C}_{2n}^-$ ($n = 1-3$), theoretical calculations were made with the Gaussian 09 program.²⁵ The structures were optimized with density functional theory (DFT) using the B3LYP functional, as this approach was widely applied in the discussion of the structure of TMC_n^- clusters.¹⁴⁻²³ The basis set of aug-cc-pVTZ was used for C and Stuttgart/Dresden (SDD) was applied to Pt (hereafter referred to as the B3LYP/aug-cc-pVTZ/SDD level of theory).²⁶ Harmonic frequency analysis ensured that the obtained structures were real minima on the potential energy surfaces and was used in the calculation of the zero-point energy (ZPE) corrections. To obtain higher precision results, the single-point energy calculations were refined at the B3LYP level in conjunction with aug-cc-pVTZ for C and aug-cc-pVTZ-PP for the Pt atom (B3LYP/aug-cc-pVTZ/aug-cc-pVTZ-PP).²⁷

Theoretically, the vertical detachment energy (VDE) was calculated as the energy difference between the neutral and the corresponding anionic species, both at the optimized anion's geometry, while the adiabatic detachment energy (ADE) was determined as the energy difference between the neutral and the anion, each at its optimized geometry, including ZPE corrections.

Moreover, to better understand the structures and stability of $\text{Pt}_2\text{C}_{2n}^-$ clusters, the chemical bondings have been analyzed using the adaptive natural density partitioning (AdNDP) method²⁸ at the B3LYP/aug-cc-pVTZ/aug-cc-pVTZ-PP level of theory.

RESULTS AND ANALYSIS

Photoelectron spectroscopy

The photoelectron imaging results of $\text{Pt}_2\text{C}_{2n}^-$ ($n = 1-3$) at 266 nm (4.661 eV) are shown in Fig. 1, where the reconstructed images (purple background) represent the central slice of the 3D laboratory frame photoelectron distribution from its 2D projection. The 355 nm experimental spectra of $\text{Pt}_2\text{C}_{2n}^-$ ($n = 1-2$) are recorded in Fig. 2 for comparison. The absence of the vibrational structure prevents us from directly measuring the ground-state ADEs, which can be estimated by drawing a straight line along the rising edge of the lowest-lying band and then adding the instrumental resolution to the intersection with the binding energy axis. In this way, the ADE values of $\text{Pt}_2\text{C}_{2n}^-$ ($n = 1-3$) are evaluated to be 2.63 ± 0.10 , 3.01 ± 0.08 , and 3.22 ± 0.07 eV (Table I), respectively. The VDEs of the ground states for $\text{Pt}_2\text{C}_{2n}^-$ ($n = 1-3$) are readily determined from the spectral peaks to be 2.84 ± 0.09 , 3.09 ± 0.08 , and

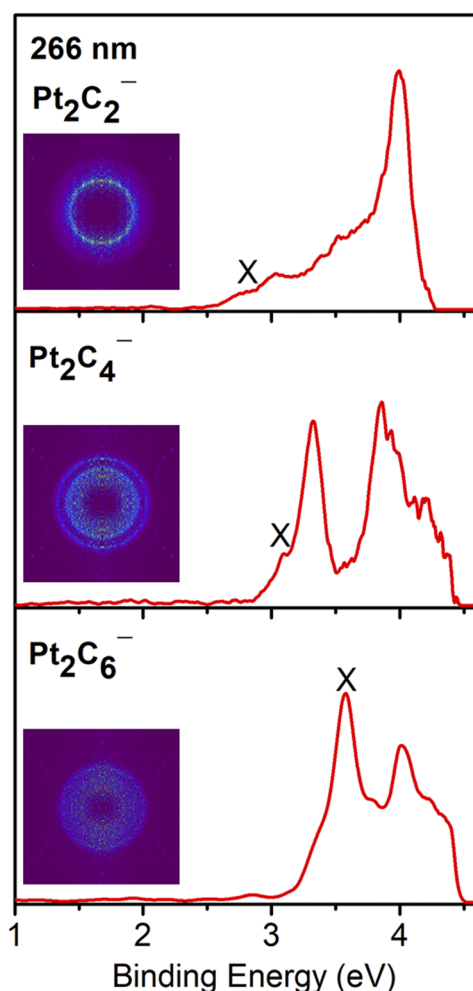


FIG. 1. Photoelectron spectra of $\text{Pt}_2\text{C}_{2n}^-$ ($n = 1-3$) recorded at 266 nm (4.661 eV). Photoelectron images after inverse Abel transformation are embedded in the photoelectron spectra.

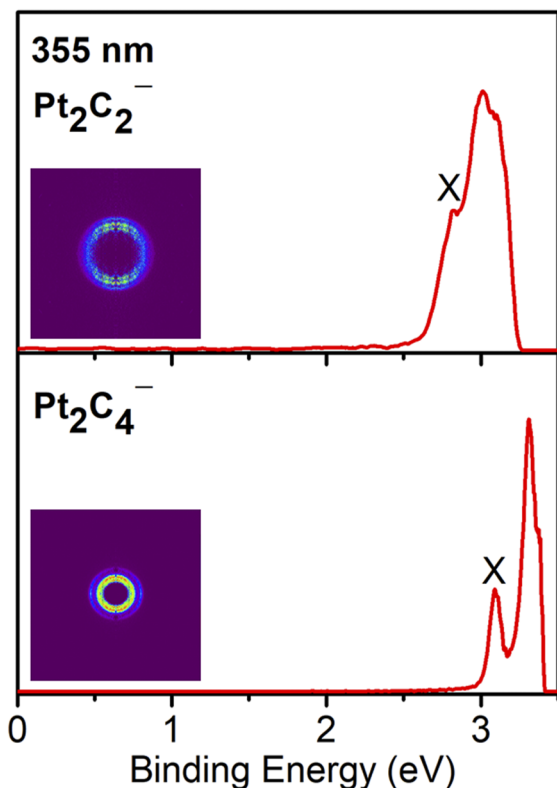


FIG. 2. Photoelectron spectra of $\text{Pt}_2\text{C}_{2n}^-$ ($n = 1-2$) recorded at 355 nm (3.496 eV). Photoelectron images after inverse Abel transformation are embedded in the photoelectron spectra.

3.58 ± 0.05 eV (Table I), respectively. Overall, the experimental VDE and ADE values increase with the growth of cluster size. β_1 of Pt_2C_4^- is 0.02 and β_2 is -0.08 in our experiment, while for Pt_2C_6^- , β_1 is -0.01 and β_2 is 0.02. The values of β_1 and β_2 are approximate, indicating the anisotropic nature of $\text{Pt}_2\text{C}_{2n}^-$ ($n = 1-3$).

Comparison between experimental and theoretical results

Quantum chemical calculations have been necessarily performed to assess the geometric and electronic structures and to help support spectral assignments. Optimized structures of low-lying isomers for $\text{Pt}_2\text{C}_{2n}^-$ ($n = 1-3$) anions and the corresponding neutrals are calculated and, respectively, displayed in Figs. 3 and 4. The theoretical VDE and ADE values of the five lowest-energy isomers for $\text{Pt}_2\text{C}_{2n}^-$ ($n = 1-3$) simultaneously computed at the B3LYP/aug-cc-pVTZ/aug-cc-pVTZ-PP level of theory are compared with the experimentally obtained data in Table I. Moreover, to further clarify the structural features, the photoelectron spectra for the theoretically calculated anionic isomers are simulated and compared with the experimental 266 nm results in Fig. 5.

Pt_2C_2^-

In Fig. 3, the lowest-lying isomer of Pt_2C_2^- (labeled 2A) is in the $D_{\infty h}$ symmetry and exhibits a linear chain Pt-C-C-Pt $^-$ structure with a $^2\Sigma_u^+$ electronic state. The 2B isomer has a C_s symmetry with two merged triangle structures and possesses a $^2A'$ electronic state. The 2B isomer lies 1.00 eV higher in energy than 2A. The 2C isomer has a $C_{\infty v}$ symmetry with an electronic state of $^4\Sigma^+$ and lies higher in energy than 2A by 1.58 eV. As listed in Table I, the calculated VDE and ADE values of 2A (2.82 and 2.75 eV) are consistent with the experimental values (2.84 ± 0.09 and 2.63 ± 0.10 eV) (Table I). By

TABLE I. Comparison of experimental VDE and ADE values to the B3LYP calculated ones of the five lowest-energy isomers for $\text{Pt}_2\text{C}_{2n}^-$ ($n = 1-3$).

Cluster	Isomer	Relative energy (eV)	VDE (eV)		ADE (eV)	
			Expt. ^a	Calc.	Expt. ^a	Calc.
Pt_2C_2^-	2A	0.00		2.82		2.75
	2B	1.00		2.60		2.32
	2C	1.58	2.84(9)	4.50	2.63(10)	4.44
	2D	1.65		3.57		3.38
	2E	1.81		1.90		1.70
Pt_2C_4^-	4A	0.00		3.17		3.08
	4B	1.21		3.20		2.72
	4C	1.33	3.09(8)	3.34	3.01(8)	2.89
	4D	1.47		4.24		3.79
	4E	1.56		3.16		2.75
Pt_2C_6^-	6A	0.00		3.44		3.33
	6B	0.65		3.61		3.56
	6C	1.05	3.58(5)	3.08	3.22(7)	2.83
	6D	1.15		3.45		3.18
	6E	1.18		3.40		3.12

^aNumbers in parentheses represent the uncertainty in the last digit.

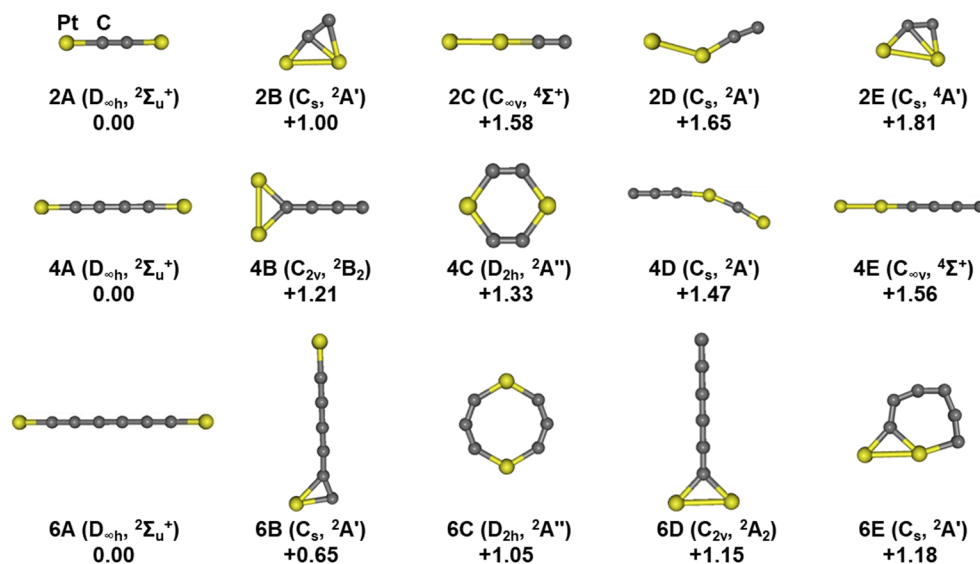


FIG. 3. Ground-state structures and selected low-lying isomers of the $\text{Pt}_2\text{C}_{2n}^-$ ($n = 1-3$) anions. Relative energies are given in eV.

contrast, the VDEs and ADEs of 2C do not match the experimental values. Moreover, the 2B and 2C isomers lie too high in energy to be experimentally probed. The simulated spectral profiles, on the other hand, provide strong evidence that the lowest-energy structure 2A contributes to this experiment (Fig. 5).

Pt_2C_4^-

For Pt_2C_4^- , the lowest-energy 4A structure has a $D_{\infty h}$ symmetry with a ${}^2\Sigma_u^+$ spin state, showing a linear chain-shaped Pt-C-C-C-Pt $^-$ geometry. The 4B isomer in the C_{2v} symmetry contains a triangle structure with a C atom connected

to three linear chain-shaped carbon atoms. The 4C isomer displays a six-member ring structure with a D_{2h} symmetry. The 4B and 4C have relative energies of 1.21 and 1.33 eV higher than 4A isomers, respectively. The calculated VDE and ADE values of 4A (3.17 and 3.08 eV) are consistent with the experiment values (3.09 ± 0.08 and 3.01 ± 0.08 eV) (Table I). The 4B isomer can be excluded, considering the marked disagreement between its simulated spectrum and the experimental result. The 4C isomer also does not exist in the present experiment, noting that its calculated VDE value (3.34 eV) is obviously higher than the experimental result (3.09 eV).

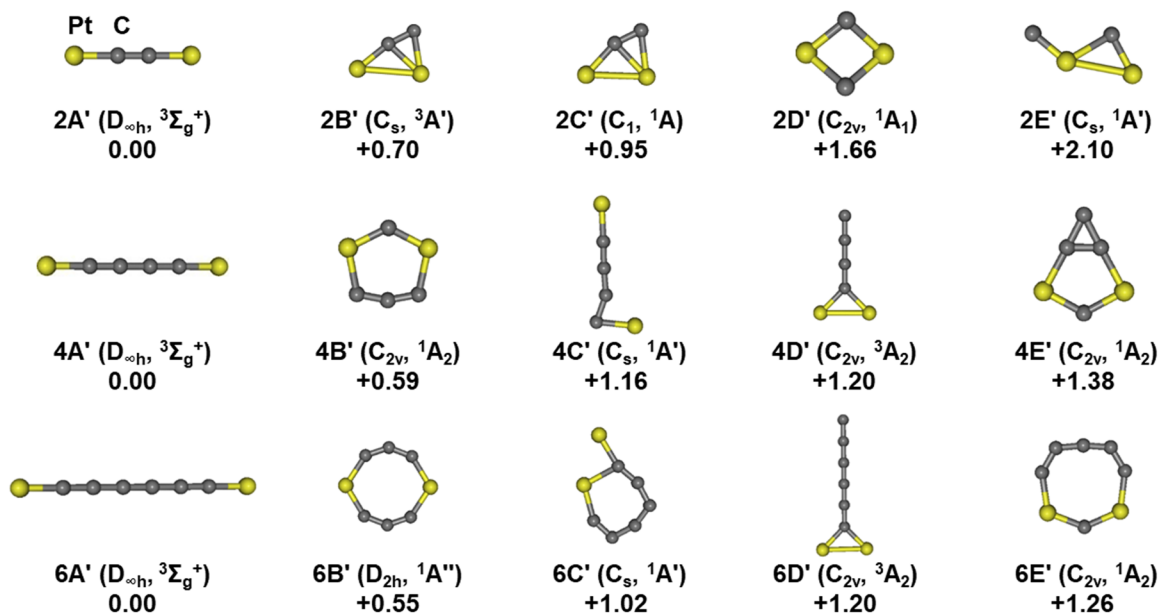


FIG. 4. Ground-state structures and selected low-lying isomers of the Pt_2C_{2n} ($n = 1-3$) neutrals. Relative energies are given in eV.

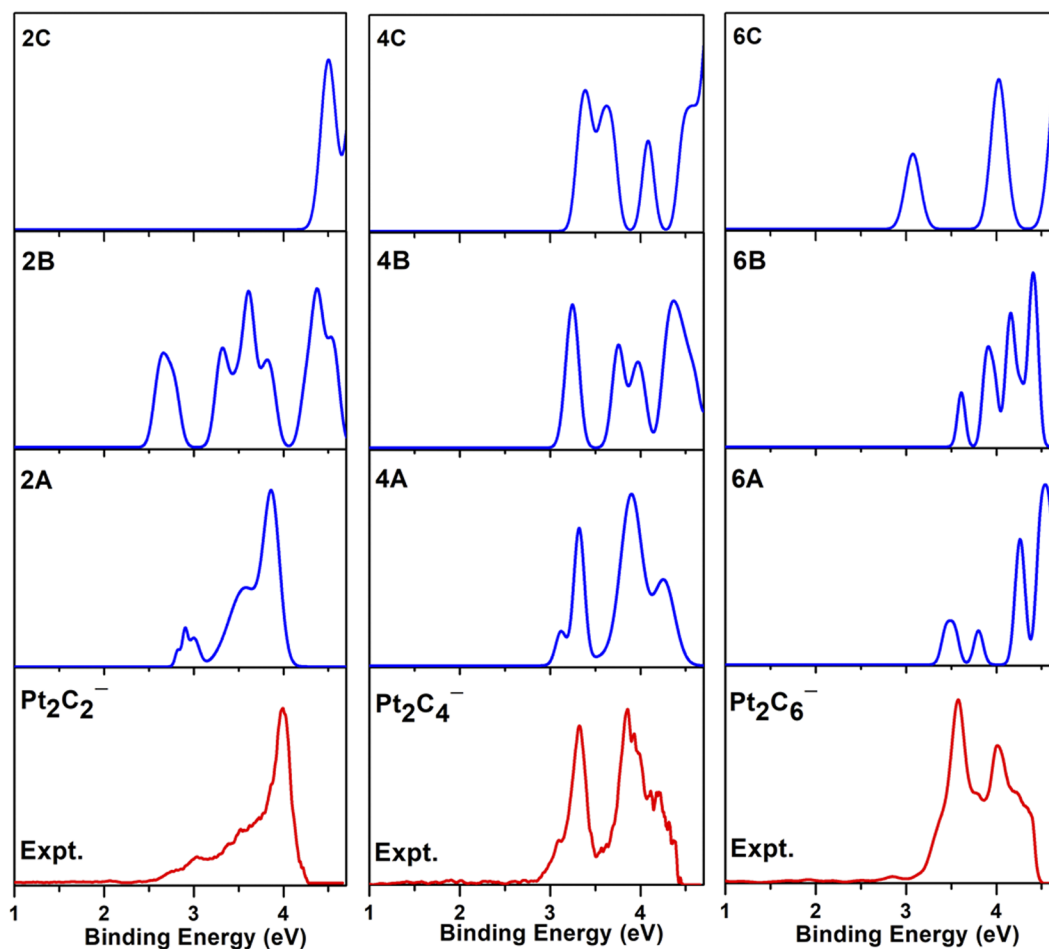


FIG. 5. Comparison of experimental 266 nm photoelectron spectra (bottom rows) of $\text{Pt}_2\text{C}_{2n}^-$ ($n = 1-3$) to the simulated spectra of the low-lying isomers (top rows).

Pt_2C_6^-

Similarly, the most stable 6A isomer of Pt_2C_6^- displays a $D_{\infty h}$ symmetry with a $^2\Sigma_u^+$ electronic state, which has a linear chain-shaped $\text{Pt}-\text{C}-\text{C}-\text{C}-\text{C}-\text{C}-\text{Pt}^-$ geometry. The 6B isomer in the $^2A'$ spin state has a triangle substructure in which one C atom is bonded to the linear $\text{C}-\text{C}-\text{C}-\text{C}-\text{Pt}$ atom chain. The 6C isomer is featured by an eight-member ring structure with a D_{2h} symmetry. The 6B and 6C isomers are higher in energy than 6A by 0.65 and 1.05 eV, respectively. The calculated VDE and ADE values of 6A (3.44 and 3.33 eV) and 6B (3.61 and 3.56 eV) agree well with the experiment values (3.58 ± 0.05 and 3.22 ± 0.07 eV) (Table I). Their simulated spectra also show good agreements with the measured curve, indicating that the 6A and 6B isomers shall coexist in the current experimental condition. The 6C–6E isomers are all excluded due to too high energy.

Pt_2C_{2n} ($n = 1-3$)

Figure 4 shows the five lowest-energy isomers of each neutral Pt_2C_{2n} ($n = 1-3$) cluster. It is worth noting that the lowest-lying isomers of neutral Pt_2C_{2n} ($n = 1-3$) all have linear chain-shaped

structures with Pt atoms distributing at both ends, which are consistent with the corresponding anions. For Pt_2C_2 , the lowest-energy $2A'$ isomer possesses a $D_{\infty h}$ structure with a $^3\Sigma_g^+$ spin state. The Pt–C bond length of Pt_2C_2 is 1.773 Å, shorter than that of Pt_2C_2^- by 0.04 Å (Fig. S1). Compared to the Pt–C bond length (2.03 Å) in polyacetylene,²⁹ the Pt–C bond length of Pt_2C_2 is shorter, which means that the Pt–C bond of Pt_2C_2 could be a double bond. In addition, the C–C bond length in Pt_2C_2 (1.289 Å) is longer than the triple bond $\text{C}\equiv\text{C}$ (1.20 Å) and shorter than single bond C–C (1.38 Å) in polyacetylene.²⁹ The bonding structure of Pt_2C_2 is more probable to be a $\text{Pt}=\text{C}=\text{C}=\text{Pt}$ configuration, which is similar to neutral O_2C_2 .³⁰ The detailed bond length values for $\text{Pt}_2\text{C}_4^{-/0}$ and $\text{Pt}_2\text{C}_6^{-/0}$ are also summarized in Fig. S1.

DISCUSSION

Figure 5 shows that the simulated spectra of the most stable isomers of the $\text{Pt}_2\text{C}_{2n}^-$ ($n = 1-3$) species agree the best with experimental spectral features, suggesting that the lowest-energy structures largely exist under the current experimental conditions. The agreement between the experimental and theoretical results allows

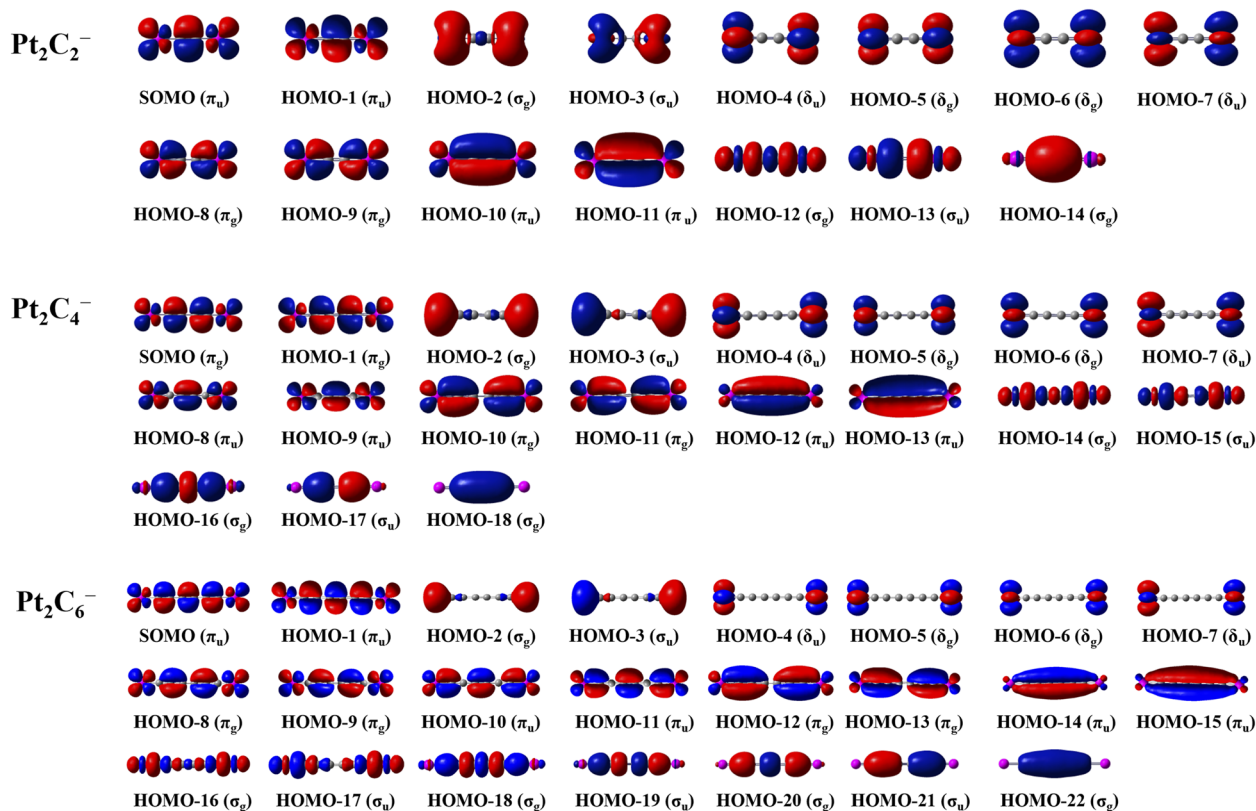


FIG. 6. The selected valence canonical molecular orbital pictures of $\text{Pt}_2\text{C}_{2n}^-$ ($n = 1-3$) ground-state anions at the B3LYP/aug-cc-pVTZ/aug-cc-pVTZ-PP level of theory.

for establishing the structural features of $\text{Pt}_2\text{C}_{2n}^-$ ($n = 1-3$). All these anionic clusters possess similar linear chain-shaped geometric configurations, which are different from the previously observed $\text{Au}_2\text{C}_{2n}^-$ ($n = 1-3$), while only metal atom substitution occurs between these cluster series.

Figure 6 displays the selected valence canonical molecular orbital pictures of $\text{Pt}_2\text{C}_{2n}^-$ ($n = 1-3$) ground-state anions. For Pt_2C_2^- , the singly occupied molecular orbital (SOMO) and HOMO-1 have C-C π bonding orbitals and Pt-C π^* anti-bonding orbitals. The detached electron should arise from HOMO-1 of $\text{Pt}_2\text{C}_{2n}^-$, leading to the $^3\Sigma_g^+$ ground state of neutral Pt-C-C-Pt. It can be seen that HOMO-4 to HOMO-7 of $\text{Pt}_2\text{C}_{2n}^-$ are all primarily 5d orbitals of Pt. Moreover, HOMO-8 and HOMO-9 of $\text{Pt}_2\text{C}_{2n}^-$ have Pt-C π orbitals and C-C π^* anti-bonding orbitals, while HOMO-10 and HOMO-11 of $\text{Pt}_2\text{C}_{2n}^-$ have Pt-C π orbitals and C-C π orbitals. By contrast, HOMO-12 of $\text{Pt}_2\text{C}_{2n}^-$ has distinct Pt-C σ bonding orbitals and HOMO-14 of $\text{Pt}_2\text{C}_{2n}^-$ has a C-C σ bond. The MOs of Pt_2C_2^- indicate two bonding orbitals (1σ and 1π), which reveals that Pt_2C_2^- has a linear cumulenic structure with a Pt=C=C=Pt configuration. It can also be found that the same bond rules from MOs of Pt_2C_4^- and Pt_2C_6^- (Fig. 6). The C-C bond lengths for $\text{Pt}_2\text{C}_{2n}^-$ ($n = 1-3$) are in the range of 1.25–1.32 Å (Fig. S1). Compared with the length of the C-C bond in polyacetylene,²⁹ the carbon chains display remarkable C-C bond length alternation with the short C-C bonds ~ 1.25 Å and

long C-C bonds about 1.32 Å, suggesting a conjugated double bond character.

The chemical bonding analyses of $\text{Pt}_2\text{C}_{2n}^-$ ($n = 1-3$) using AdNDP are indicated in Fig. 7. It can be seen readily that two Pt-C bonds and two C-C bonds exist in the Pt_2C_2^- anion besides eight 5d lone pairs of Pt atoms. For Pt_2C_2^- , there are three two-center two-electron ($2c-2e$) σ bonds (two $2c-2e$ Pt-C σ bonds and one $2c-2e$ C-C σ bond) and three $2c-2e$ π bonds (two $2c-2e$ Pt-C π bonds and single $2c-2e$ C-C π bond). Interestingly, it has one $4c-1e$ bond, which is traced to the SOMO of Pt_2C_2^- in Fig. 6. This also shows that Pt_2C_2^- has a Pt=C=C=Pt structure.

Pt_2C_4^- has two Pt-C bonds and three C-C bonds besides eight 5d lone pairs of Pt atoms, whereas there are five two-center two-electron ($2c-2e$) σ bonds, including three C-C σ bonds and two Pt-C σ bonds, and four $2c-2e$ π bonds, including two $2c-2e$ Pt-C π bonds and two C-C π bonds. In addition, it also has one $4c-2e$ C-C-C-C π bond. Moreover, it also has one $6c-1e$ bond, which is traced to the SOMO of Pt_2C_4^- in Fig. 6. For Pt_2C_6^- , it has two Pt-C bonds and five C-C bonds besides eight 5d lone pairs of Pt atoms, whereas there are seven $2c-2e$ σ bonds involving five C-C σ bonds and two Pt-C σ bonds. It has two $2c-2e$ Pt-C π bonds and many characters of $2c-2e$ C-C π bonds. In addition, it has two $4c-2e$ C-C-C-C π bonds. Furthermore, there is also one $8c-1e$ bond, which is also traced to the SOMO of Pt_2C_6^- in Fig. 6. It shows that $\text{Pt}_2\text{C}_{2n}^-$ ($n = 1-3$) have

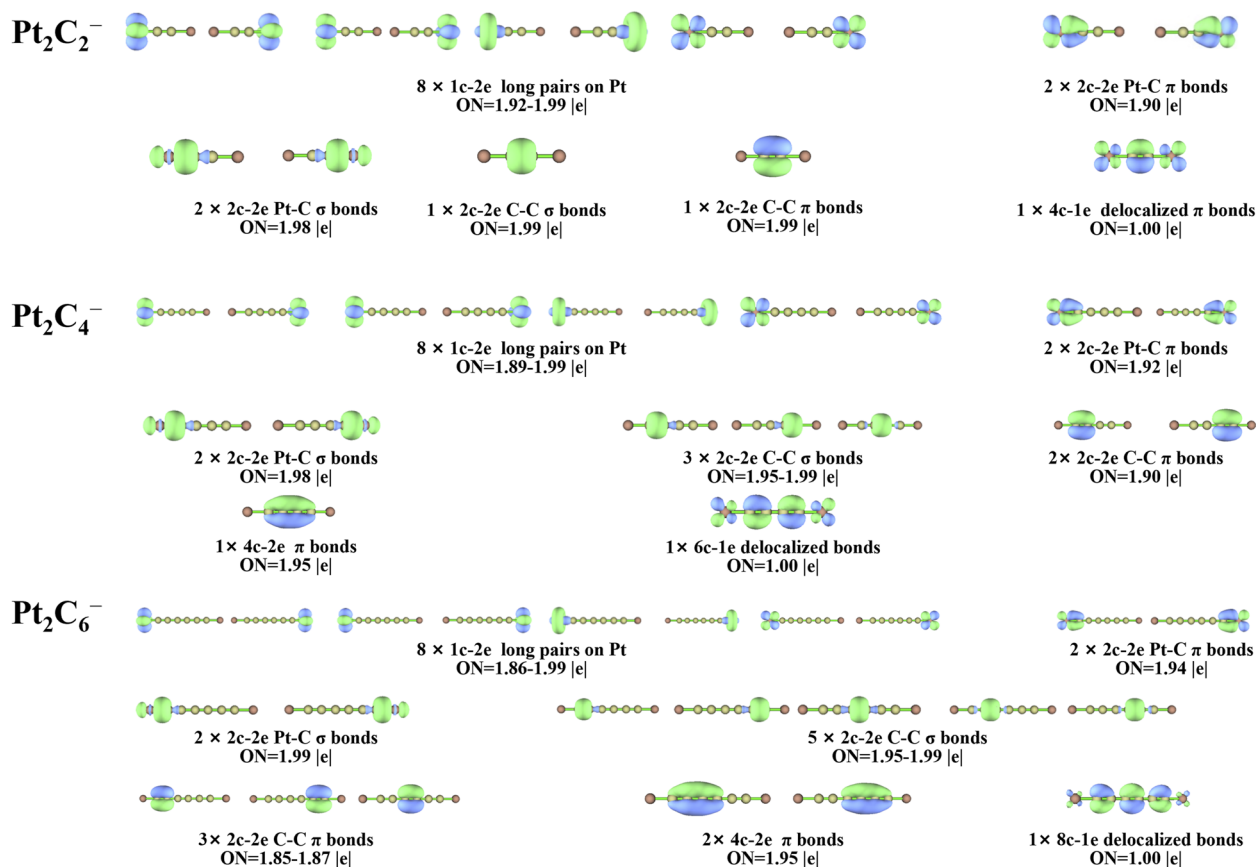


FIG. 7. Chemical bonding analyses of Pt₂C_{2n}⁻ (n = 1–3) using Adaptive Natural Density Partitioning (AdNDP) at the B3LYP/aug-cc-pVTZ/aug-cc-pVTZ-PP level of theory.

the same feature as platinum ethene [Pt=(C=C)_nPt⁻] from Figs. 6 and 7.

CONCLUSION

The Pt₂C_{2n}⁻ (n = 1–3) cluster anions were generated via a laser vaporization supersonic cluster source and characterized by mass-selected time-of-flight photoelectron velocity-map imaging spectroscopy. Theoretical calculations were performed to elucidate the geometric and electronic structures. The experimental and calculated results reveal that the binding motif in the most stable isomer of Pt₂C₂⁻, a linear cumulenic structure with a Pt=C=C=Pt configuration, is restrained in the lowest-energy isomers for both the Pt₂C₄⁻ and Pt₂C₆⁻ anions [Pt=(C=C)_nPt⁻]. The chemical bonding analyses indicate that Pt₂C_{2n}⁻ (n = 1–3) has multicenter two-electron features with strong electron delocalization.

SUPPLEMENTARY MATERIAL

See the [supplementary material](#) for detailed information on structures and bond lengths of the most stable isomers for Pt₂C_{2n}^{-/0} (n = 1–3).

ACKNOWLEDGMENTS

This work was supported by the National Natural Science Foundation of China (Grant Nos. 21973084, 21688102, and 21873097), the Youth Innovation Promotion Association of the Chinese Academy of Sciences (CAS) (Grant No. 2020187), the Strategic Priority Research Program of CAS (Grant No. XDB17000000), the CAS (Grant No. GJJSTD20190002), the International Partnership Program of CAS (Grant No. 121421KYSB20170012), and the K. C. Wong Education Foundation (Grant No. GJTD-2018-06). The authors acknowledge the Dalian Coherent Light Source (DCLS) for support and assistance.

AUTHOR DECLARATIONS

Conflict of Interest

The authors have no conflicts to disclose.

DATA AVAILABILITY

The data that support the findings of this study are available within the article and its [supplementary material](#).

REFERENCES

- ¹B. Qiao, A. Wang, X. Yang, L. F. Allard, Z. Jiang, Y. Cui, J. Liu, J. Li, and T. Zhang, *Nat. Chem.* **3**, 634 (2011).
- ²R. Lang, X. Du, Y. Huang, X. Jiang, Q. Zhang, Y. Guo, K. Liu, B. Qiao, A. Wang, and T. Zhang, *Chem. Rev.* **120**, 11986 (2020).
- ³L. Zhang, M. Zhou, A. Wang, and T. Zhang, *Chem. Rev.* **120**, 683 (2020).
- ⁴B. Han, Y. Guo, Y. Huang, W. Xi, J. Xu, J. Luo, H. Qi, Y. Ren, X. Liu, B. Qiao, and T. Zhang, *Angew. Chem., Int. Ed.* **59**, 11824 (2020).
- ⁵G. Vilé, D. Albani, M. Nachttegaal, Z. Chen, D. Dontsova, M. Antonietti, N. López, and J. Pérez-Ramírez, *Angew. Chem., Int. Ed.* **54**, 11265 (2015).
- ⁶T. Whittaker, K. B. S. Kumar, C. Peterson, M. N. Pollock, L. C. Grabow, and B. D. Chandler, *J. Am. Chem. Soc.* **140**, 16469 (2018).
- ⁷T. He, W. Wang, F. Shi, X. Yang, X. Li, J. Wu, Y. Yin, and M. Jin, *Nature* **598**, 76 (2021).
- ⁸S. T. Hunt, M. Milina, A. C. Alba-Rubio, C. H. Hendon, J. A. Dumesic, and Y. Roman-Leshkov, *Science* **352**, 974 (2016).
- ⁹A. T. Bell, *Science* **299**, 1688 (2003).
- ¹⁰L. Zhang, L. T. Roling, X. Wang, M. Vara, M. Chi, J. Liu, S.-I. Choi, J. Park, J. A. Herron, Z. Xie, M. Mavrikakis, and Y. Xia, *Science* **349**, 412 (2015).
- ¹¹P. Pyykkö, *Angew. Chem., Int. Ed.* **43**, 4412 (2004).
- ¹²D. M. Bittner, D. P. Zaleski, D. P. Tew, N. R. Walker, and A. C. Legon, *Angew. Chem., Int. Ed.* **55**, 3768 (2016).
- ¹³Q. Zhang, L.-c. Song, X. Lu, R.-b. Huang, and L.-S. Zheng, *J. Mol. Struct.* **967**, 153 (2010).
- ¹⁴B. R. Visser, M. A. Addicoat, J. R. Gascooke, W. D. Lawrance, and G. F. Metha, *J. Chem. Phys.* **138**, 174310 (2013).
- ¹⁵I. León, Z. Yang, and L.-S. Wang, *J. Chem. Phys.* **140**, 084303 (2014).
- ¹⁶I. León, F. Ruipérez, J. M. Ugalde, and L. S. Wang, *J. Chem. Phys.* **145**, 064304 (2016).
- ¹⁷P. Wang, W. Zhang, X.-L. Xu, J. Yuan, H.-G. Xu, and W. Zheng, *J. Chem. Phys.* **146**, 194303 (2017).
- ¹⁸I. León, F. Ruipérez, J. M. Ugalde, and L.-S. Wang, *J. Chem. Phys.* **149**, 144307 (2018).
- ¹⁹X. Sun, J. Du, and G. Jiang, *Struct. Chem.* **24**, 1289 (2012).
- ²⁰Y. Wei, J. X. Xu, X. M. Yuan, and X. H. Zheng, *Adv. Mater. Res.* **652–654**, 815 (2013).
- ²¹S.-J. Lu, *Chem. Phys. Lett.* **694**, 70 (2018).
- ²²S.-J. Lu, *Chem. Phys. Lett.* **699**, 218 (2018).
- ²³S.-J. Lu, X.-L. Xu, H.-G. Xu, and W.-J. Zheng, *J. Chem. Phys.* **151**, 224303 (2019).
- ²⁴Z. Qin, X. Wu, and Z. Tang, *Rev. Sci. Instrum.* **84**, 066108 (2013).
- ²⁵M. J. Frisch, G. W. Trucks, H. B. Schlegel, G. E. Scuseria, M. A. Robb, J. R. Cheeseman, G. Scalmani, V. Barone, B. Mennucci, G. A. Petersson, H. Nakatsuji, M. Caricato, X. Li, H. P. Hratchian, A. F. Izmaylov, J. Bloino, G. Zheng, J. L. Sonnenberg, M. Hada, M. Ehara, K. Toyota, R. Fukuda, J. Hasegawa, M. Ishida, T. Nakajima, Y. Honda, O. Kitao, H. Nakai, T. Vreven, J. A. Montgomery, Jr., J. E. Peralta, F. Ogliaro, M. J. Bearpark, J. Heyd, E. N. Brothers, K. N. Kudin, V. N. Staroverov, R. Kobayashi, J. Normand, K. Raghavachari, A. P. Rendell, J. C. Burant, S. S. Iyengar, J. Tomasi, M. Cossi, N. Rega, N. J. Millam, M. Klene, J. E. Knox, J. B. Cross, V. Bakken, C. Adamo, J. Jaramillo, R. Gomperts, R. E. Stratmann, O. Yazyev, A. J. Austin, R. Cammi, C. Pomelli, J. W. Ochterski, R. L. Martin, K. Morokuma, V. G. Zakrzewski, G. A. Voth, P. Salvador, J. J. Dannenberg, S. Dapprich, A. D. Daniels, O. Farkas, J. B. Foresman, J. V. Ortiz, J. Cioslowski, and D. J. Fox, Gaussian 09, Gaussian, Inc., Wallingford, CT, 2009.
- ²⁶M. Dolg, H. Stoll, and H. Preuss, “Energy adjusted *ab initio* pseudopotentials for the rare earth elements,” *J. Chem. Phys.* **90**, 1730 (1989).
- ²⁷T. H. Dunning, *J. Chem. Phys.* **90**, 1007 (1989).
- ²⁸D. Y. Zubarev and A. I. Boldyrev, *Phys. Chem. Chem. Phys.* **10**, 5207 (2008).
- ²⁹Q. Zheng, J. C. Bohling, T. B. Peters, A. C. Frisch, F. Hampel, and J. A. Gladysz, *Chem. - Eur. J.* **12**, 6486 (2006).
- ³⁰A. R. Dixon, T. Xue, and A. Sanov, *Angew. Chem., Int. Ed.* **54**, 8764 (2015).